Inorganic Chemistry

Article

pubs.acs.org/IC

Electronic Effects on a Mononuclear Co Complex with a Pentadentate Ligand for Catalytic H_2 Evolution

Manohar Vennampalli, Guangchao Liang,[‡] Lakshmi Katta, Charles Edwin Webster,*[,‡] and Xuan Zhao*

Department of Chemistry, The University of Memphis, Memphis, Tennessee 38152, United States

Supporting Information

ABSTRACT: Previous studies of Co catalysts for H_2 evolution have shown opposite effects between the redox potentials of Co centers and their catalytic properties such as the overpotential and turnover frequency: Co catalysts with more positive reduction potentials from structural modification display insignificant changes in the overpotential for H_2 evolution and require stronger acid for catalysis, and Co catalysts with lower overpotentials show decreased turnover frequency for H_2 evolution. In order to explore the electronic effects of a ligand scaffold on the catalytic properties for H_2 evolution by a Co complex with a pentadentate ligand, *N*,*N*-bis(2-pyridinylmethyl)-2,2′-bipyridine-6-methanamine (DPA-Bpy), we replaced the pyridyls in DPA-Bpy with more basic isoquinoline groups. In contrast to data from previously reported studies, in the current study, a Co complex with a more positive reduction potential, resulting from the replacement of pyridyls with isoquinoline groups, leads to a lower overpotential and higher turnover frequency for both electro- and photocatalytic H_2 production in neutral aqueous solution.

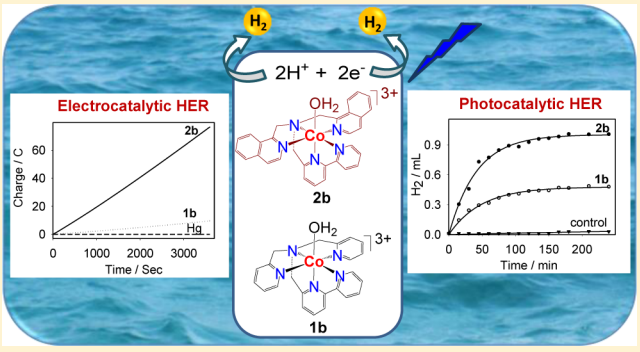

INTRODUCTION

The potential use of H_2 as a clean and renewable source of energy requires the discovery of new catalysts for the production of H_2.[1] Catalysts for H_2 production, especially those based on earth-abundant metals such as Ni, Co, and Fe, have been extensively studied over the past years.[2] The design of catalysts that operate in aqueous solution for the electro- and photochemical production of H_2 represents a great challenge for future applications.[3] For example, Co complexes based on tetra- and pentadentate ligands have been reported for the catalytic production of H_2 in aqueous solution.[3a,b,4]

Previous studies of Co catalysts have provided important insight into the structure−function relationship of catalytic properties such as the overpotential and turnover frequency (TOF) for H_2 evolution.[5] Structural modifications of Co catalysts for H_2 production demonstrated that the tuning of the Co center to a more positive reduction potential with electron-withdrawing groups results in an insignificant decrease in the overpotential, while electron-donating groups on the axial ligand trans to the Co−H species could greatly enhance the catalytic current for H_2 production because of the formation of more basic Co−H species.[5,6] For example, from voltammetric simulations, Artero and co-workers reported an increase of 40-fold and a decrease of 5-fold in the rate of H_2 evolution by cobaloxime catalysts when an electron-donating dimethylamino and an electron-withdrawing *N*-*tert*-butylamido substituent were introduced, respectively, in the para position of the axial pyridine ligand.[6a] Furthermore, it has been shown that ligand modification in Co-containing catalysts that lower the overpotential leads to a decrease in the TOF for H_2 evolution.[7]

We reported the synthesis and characterization of mononuclear Co complexes, [Co(DPA-Bpy)Cl]Cl (**1a**) and [Co(DPA-Bpy)(H_2O)](PF_6)$_3$ (**1b**), where DPA-Bpy = *N*,*N*-bis(2-pyridinylmethyl)-2,2′-bipyridine-6-methanamine, and investigated the activity of **1b** for electro- and photocatalytic H_2 evolution in aqueous solution (Figure 1).[8] Complex **1b** catalyzes electrolytic H_2 evolution with an overpotential of 600 mV in a pH 7 buffer.

In comparison to pyridine, which has a pK_a of 5.22, isoquinoline is more basic with pK_a of 5.46 because of the resonance and inductive effects of the additional benzene group.[9] In order to investigate the electronic effects of a ligand

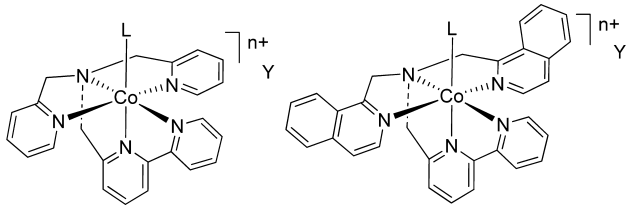

1a; n = 1, L = Cl^-, Y = Cl^-
1b; n = 3, L = OH_2, Y = $(PF_6^-)_3$

2a; n = 1, L = Cl^-, Y = Cl^-
2b; n = 3, L = OH_2, Y = $(PF_6^-)_3$

Figure 1. Mononuclear Co complexes.

Received: April 9, 2014
Published: September 23, 2014

dx.doi.org/10.1021/ic500840e | *Inorg. Chem.* 2014, 53, 10094−10100

scaffold and in an effort to improve the catalytic properties of **1b** for H_2 evolution, we replaced the pyridyls in DPA-Bpy with more basic and more conjugated isoquinoline groups to yield new Co complexes, [Co(DIQ-Bpy)Cl]Cl (**2a**) and [Co(DIQ-Bpy)(H_2O)](PF_6)$_3$ (**2b**), where DIQ-Bpy = *N*,*N*-bis-((isoquinolin-1-yl)methyl)(6-(pyridin-2-yl)pyridin-2-yl)-methanamine (Figure 1). In contrast to what has been observed for cobaloxime catalysts, we report here that **2b** displays much higher activity than **1b** in both electro- and photocatalytic H_2 production. The more positive reduction potential of the Co center in **2b** results in a significantly lower overpotential and higher TOF, as well as enhanced stability for electrolytic H_2 evolution in neutral aqueous solution.

EXPERIMENTAL SECTION

All chemicals were purchased from Sigma-Aldrich and Alfa-Aesar except as noted. Other reagents such as 1-methylisoquinoline, $CoCl_2 \cdot 6H_2O$, and 2,2′-dipyridyl were used as received without further purification. Milli-Q water (18.2 MΩ) was used in all experiments. Syntheses of (bromomethyl)isoquinoline and 6-(aminomethyl)-2,2′-bipyridine were carried out following literature methods.[10] Co(CH_3CN)$_6$(PF_6)$_2$ was prepared using a reported procedure.[11] The synthesis of *N*,*N*-bis[(isoquinolin-1-yl)methyl][6-(pyridin-2-yl)-pyridin-2-yl]methanamine (DIQ-Bpy) was accomplished as described in the literature.[12]

UV−vis absorption spectra were measured with a HP-8452A diode-array spectrometer. Electrospray ionization mass spectrometry (ESI-MS) spectra were obtained from a Thermo Electron LCQ Advantage liquid chromatograph−mass spectrometer. Elemental analyses were done by Atlantic Microlab, Inc., Atlanta, GA. All of the experiments were conducted under an Ar atmosphere unless noted otherwise. The amount of H_2 produced was determined by gas chromatography using a HP 5890 series II gas chromatograph with a thermal conductivity detector (molecular sieve 5 Å column).

Cyclic voltammetry (CV) measurements were performed with a CH Instruments potentiostat (model 660) in 0.1 M tetrabutylammonium hexafluorophosphate (Bu_4NPF_6) in acetonitrile using ferrocene (Fc; $E_{1/2}$ = 0.64 V vs SHE) as an internal reference.[13] A 0.1 M Britton−Robinson buffer or a 1.0 M pH 7.0 sodium phosphate buffer was used with glassy carbon or a BASi controlled-growth mercury electrode as the working electrode, Pt wire as the counter electrode, and Ag/AgCl as the reference electrode in 3 M KCl and 0.1 M NBu_4PF_6 in acetonitrile for aqueous and nonaqueous solution, respectively. Following literature protocol, controlled potential electrolysis was conducted in an H-type gastight dual-compartment cell in a 1.0 M sodium phosphate buffer at pH 7.[8b] Faradaic efficiencies of H_2 production at a 50 μM catalyst were determined at applied potentials of −1.2, −1.3, and −1.4 V vs SHE. The volume of H_2 produced during electrolysis was determined by a gas buret. The electrolysis experiments were performed at 22 °C, and the vapor pressure of water at 22 °C (19.8 mmHg) was corrected in calculating the current efficiency of H_2 production.

Synthesis of [Co(DIQ-Bpy)Cl]Cl·H_2O (2a·H_2O). To a Schlenk flask containing a degassed solution of DIQ-Bpy (0.2 g, 0.428 mmol) in CH_3CN (50 mL) was added dropwise a 50 mL CH_3CN solution of $CoCl_2 \cdot 6H_2O$ (0.102 g, 0.428 mmol) through an addition funnel. The reaction mixture was stirred overnight at room temperature under an Ar atmosphere. The resultant reaction mixture was filtered through Celite under an Ar atmosphere using a cannula, and the solvent was removed under reduced pressure. The resulting brownish-orange solid was dissolved in a minimum amount of degassed methanol and precipitated with degassed diethyl ether. After removal of ether, the resulting precipitate was washed with ether a few times to yield complex **2a** as a brownish-orange solid (0.24 g, 94%). ESI-MS: *m*/*z* 561.11 (calcd *m*/*z* 561.30 for [Co(DIQ-Bpy)Cl]$^+$). Anal. Calcd for $C_{31}H_{25}Cl_2CoN_5 \cdot H_2O$: C, 60.50; H, 4.42; N, 11.38. Found: C, 60.76; H, 4.49; N, 11.29. Absorption maxima (λ_{max}, nm): 305, 387 (br).

Synthesis of [Co(DIQ-Bpy)(OH_2)](PF_6)$_3$·2H_2O (2b·2H_2O). To a solution of **2a** (0.15 g, 0.25 mmol) in 20 mL of water was added dropwise a solution of $AgPF_6$ (0.22 g, 0.84 mmol) in 10 mL of water under an Ar atmosphere. The reaction mixture was refluxed for 12 h. After the precipitate was filtered through Celite, water was removed under reduced pressure, and the residue was dissolved in a minimum amount of methanol, washed with diethyl ether, and dried under vacuum to produce a pinkish-yellow solid as complex **2b** (0.19 g, 77%). ^{1}H NMR (D_2O, 500 MHz): δ 5.72 (s, 2H, bipyridyl methylene H8), 6.03 (d, *J* = 16.8 Hz, 2H, axial isoquinoline methylene H1), 6.11 (d, *J* = 16.8 Hz, 2H, equatorial isoquinoline methylene H1), 6.74 (d, *J* = 6.6 Hz, 2H, iq-H6), 7.39 (d, *J* = 7.9 Hz, 1H, bpy-H9), 7.70 (d, *J* = 6.6 Hz, 2H, iq-H7), 7.84 (t, *J* = 7.0 Hz, 2H, iq-H4), 7.90 (d, *J* = 8.2 Hz, 2H, iq-H2), 7.94 (d, *J* = 7.0 Hz, 2H, iq-H5), 8.08 (t, *J* = 7.9 Hz, 1H, bpy-H10), 8.21 (t, *J* = 8.2 Hz, 2H, iq-H3), 8.22 (t, *J* = 4.9 Hz, 1H, bpy-H14), 8.40 (d, *J* = 7.9 Hz, 1H, bpy-H11), 8.73 (t, *J* = 7.8 Hz, 1H, bpy-H13), 8.84 (d, *J* = 8.1 Hz, 1H, bpy-H12), 8.98 (d, *J* = 4.9 Hz, 1H, bpy-H15). ESI-MS: *m*/*z* 688.28 (calcd *m*/*z* 688.11 for [Co(DIQ-Bpy)(OH)(PF_6)]$^+$). Anal. Calcd for $C_{31}H_{27}CoF_{18}N_5OP_3 \cdot 2H_2O$: C, 36.67; H, 3.08; N, 6.90. Found: C, 36.58; H, 3.13; N, 6.70. Absorption maxima (λ_{max}, nm): 305, 468.

General Procedure for Photocatalytic H_2 Production. For photocatalytic H_2 evolution, each sample was prepared in a 130 mL rectangular flask containing 10 mL of a 1.0 M pH 5.0 acetate buffer in the presence of photosensitizer [Ru(bpy)$_3$]Cl_2 (0.5 mM) and sacrificial electron-donor ascorbic acid (0.1 M). The reaction flask was sealed with a septum, degassed under vacuum, and flushed with Ar gas to remove any oxygen present in the flask. After the addition of a catalyst (5.0 μM), the flask was degassed again before irradiation. The samples were irradiated by LED light (Cree 3-Up XP-E, 450 nm) at room temperature (22 °C) at constant stirring.

The photolysis experiment to investigate the decomposition process by ESI-MS was carried out in a solution containing 50.0 μM **1b**, ascorbic acid (0.1 M), and [Ru(bpy)$_3$]$^{2+}$ (0.5 mM) in a 1.0 M ammonium acetate buffer (pH 5) under irradiation by LED light (Cree 3-Up XP-E, 450 nm). Before and after photolysis at certain time intervals, the photolysis solution was taken by a syringe and extracted with dichloromethane. Upon removal of dichloromethane under vacuum and dissolution in methanol, the resulting solution was analyzed by ESI-MS.

Density Functional Theory (DFT) Calculations. All DFT computations were performed using a pure functional: PBEPBE[14] (the 1996 exchange and gradient-corrected correlation functionals of Perdew, Burke, and Ernzerhof) via the *Gaussian 09*[15] software package, version C01. In basis set 1 (BS1), the Co atom used the effective core potential and associated basis set of the Couty and Hall modified LANL2DZ[16] and all other atoms used the 6-31G (d′)[17,18] basis sets. All geometries are fully optimized and confirmed as minima by analytical vibrational frequency calculations with PBEPBE/BS1. The density fitting approximation, via the keyword AUTO, for the fitting of the Coulomb potential was used for all computations. The SMD[19] continuum solvation model via the self-consistent reaction field (SCRF) keyword was used to approximate the solvation effects associated with water as solvent. Computations of the solvation energy were carried out from single-point calculations on gas-phase-optimized geometries with default parameters. The thermodynamic Born−Haber cycle was used to calculate the one-electron redox potentials of Co complexes based on the computational results of reduced and oxidized forms of Co complexes (Scheme 1).

$$E_{rxn} = \frac{-\Delta G_{rxn}}{nF} - \text{SHE} \quad (1)$$

where the change of the Gibbs free energy of the redox half-reaction in solution, ΔG_{rxn}, consists of the free energy change in the gas phase (ΔG_{GP}) and the solvation free energies of the oxidized and reduced species ($-\Delta G_{Ox,solv}$ and $-\Delta G_{Red,solv}$, respectively). *F* is the Faraday constant, namely, 23.06 kcal mol^{-1} V^{-1}, and *n* is the number of electrons in the reaction (eq 1). The experimental value[21] for the solvation of a proton in water ($\Delta G_{H^+,solv,water}$ = −265.9 kcal mol^{-1}) was used to account for the loss of a proton to solvent water. The

dx.doi.org/10.1021/ic500840e | Inorg. Chem. 2014, 53, 10094−10100

Scheme 1. Thermodynamic Cycle[20] Used To Calculate the Redox Potentials

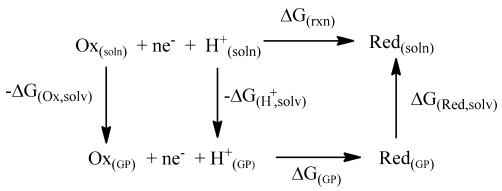

experimental value,[22] −6.28 kcal mol^{-1}, was used as the gas-phase Gibbs free energy of a proton ($\Delta G_{H^+,GP}$). While the most frequently cited experimental value for the absolute standard hydrogen electrode (SHE) is 4.44 V, the PBEPBE/BS1 DFT-computed value for the absolute redox potential of SHE is 4.02 V, and this value was used as a reference for the redox potential of Co complexes.

RESULTS AND DISCUSSION

Synthesis and Characterization. Mononuclear Co complexes **2a** and **2b** were prepared following the literature method for the synthesis of **1a** and **1b** (Scheme 2).[8b] The reaction of DIQ-Bpy with $CoCl_2 \cdot 6H_2O$ in acetonitrile led to the formation of **2a** as a brownish-orange powder, which can be converted to **2b** by refluxing with excess $AgPF_6$ in aqueous solution.[8b,12] Both **2a** and **2b** have been characterized by UV−vis, mass spectrometry, and elemental analysis.

The ^{1}H NMR spectrum of **2b**, as shown in Figure S1 in the Supporting Information (SI), suggests the presence of a diamagnetic low-spin Co^{III} center. The two isoquinoline groups in **2b** display the same NMR features, suggesting the presence of C_s symmetry with a plane containing the tertiary amine and the bipyridine group in solution. These structural features of **2b** are similar to those of **1b** and agree with the optimized structure of **2b** from DFT computations (Figure 2).[8b] Compared to the free DIQ-Bpy ligand, coordination of the Co ion resulted in the downfield shifts of all three methylene groups, H2−H5, and H6−H15 in **2b** (Figure S1 and Table S1 in the SI).[12] Complex **2a** shows absorption at 305 nm and a broad peak at 387 nm, while **2b** displays absorption at 305 nm and a less intense peak at 468 nm, characteristic of the $Co^{III}OH_2$ form (Figure S2 in the SI). The pK_a value of the coordinated water in **2b** was determined to be 5.9 by fitting the UV−vis absorbance changes at 468 and 480 nm in the range of pH 2−8.6 (Figure S3 in the SI).[8a,b]

Electrochemical Studies. The cyclic voltammogram of **2a** in CH_3CN displays three reversible redox potentials at 0.30, −0.90, and −1.36 V (vs SHE), assignable to $Co^{III/II}$, $Co^{II/I}$, and $Co^{I/0}$, respectively (Figure S4 in the SI). One additional redox event was observed at more negative potential at −1.56 V (vs SHE), possibly arising from ligand-based reduction (Figure S4 in the SI). The DIQ-Bpy ligand displays an irreversible reduction at −1.99 V (vs SHE) in the same region (Figure S4c in the SI). Under the same conditions, **1a** displays redox

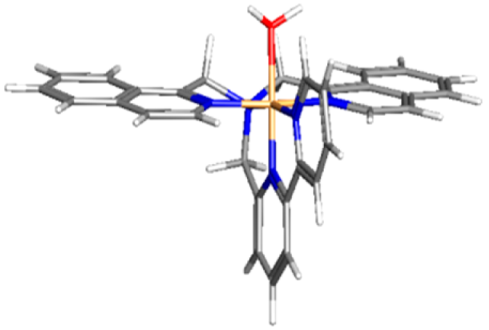

Figure 2. DFT-optimized structure of the cationic moiety of **2b**. Color code: yellow, Co; blue, N; red, O; gray, C; white, H.

potentials at +0.35, −0.94, −1.53, and −1.86 V, while the DPA-Bpy ligand shows an irreversible reduction at −1.96 V (vs SHE; Figure S5 in the SI).[8b] The reversibility of the $Co^{III/II}$ couple of both **1a** and **2a** indicates the possibility that the Cl ion remains coordinated to the Co^{II} center, as has been suggested from the chloride effect on the activity of cobalt polypyridine complexes for H_2 evolution.[23]

Because of the more basic isoquinoline groups, the $Co^{III/II}$ couple of **2a** occurs at a less positive redox potential than that of **1a**. In contradiction to that predicted based on the more electron-donating isoquinoline groups, the redox potentials of both the $Co^{II/I}$ and $Co^{I/0}$ couples of **2a** are more positive than those of **1a**. Previous studies have shown that an extended conjugated ligand could help to stabilize low-valent Co centers, resulting in higher redox potentials of the Co center.[2f] Therefore, except for the $Co^{III/II}$ couple, the substitution of pyridyls in DPA-Bpy with isoquinoline groups in DIQ-Bpy results in positive shifts of the redox potentials of **2a**.

The redox properties of **2b** were investigated in aqueous solution at different pHs. As shown in Figure S6 in the SI, the Pourbaix diagram[24] of the $Co^{III/II}$ couple shows a pH-dependent redox potential change from pH 6 to pH 11.8 with a slope of 49.9 mV pH^{-1}, consistent with a proton-coupled electron-transfer process ($Co^{III}OH + H^+ + e^- \rightarrow Co^{II}OH_2$). At pH < 6 and pH > 11.8, the $Co^{III/II}$ couple remains nearly unchanged, corresponding to the redox processes of $Co^{III}OH_2 + e^- \rightarrow Co^{II}OH_2$ and $Co^{III}OH + e^- \rightarrow Co^{II}OH$, respectively. From the Pourbaix diagram, the pK_a values of $Co^{III}OH_2$ and $Co^{II}OH_2$ species can be derived as 5.9 and 11.8, respectively. At pH 7, the $Co^{III/II}$ couple of **2b** has a redox potential of 0.14 V (vs SHE), nearly the same as that of **1b** (Table 1). When a controlled-growth mercury electrode was used as the working electrode, the cyclic voltammogram of **2b** shows a redox potential at −0.73 V (vs SHE), corresponding to the $Co^{II/I}$ couple. The more negative potential at −0.82 V (vs SHE), after the formation of Co^I species, was tentatively assigned as the $Co^{III}H/Co^{II}H$ couple (Figure 3), while we could not rule out the possibility of the reduction of Co^I to Co^0 or ligand-based

Scheme 2. Synthesis of Co Complexes

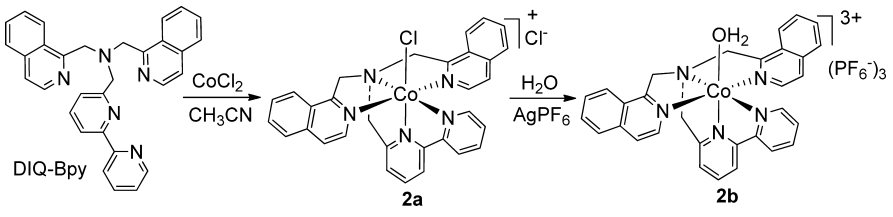

dx.doi.org/10.1021/ic500840e | Inorg. Chem. 2014, 53, 10094−10100

Table 1. Experimental and Computed Redox Potentials of 1b and 2b in Water at pH 7, $E_{1/2}$, V vs SHE

	$Co^{III/II}$ [a]	$Co^{III/II}$ [b]	$Co^{II/I}$ [c]	$Co^{II/I}$ [b]	$Co^{III}H/Co^{II}H$ [c]	$Co^{III}H/Co^{II}H$ [b]
1b	0.15	0.09	−0.84	−0.68	−0.96	−0.74
2b	0.14	−0.03	−0.73	−0.59	−0.82	−0.73

[a]Glassy carbon electrode. [b]Computed redox potential. [c]Mercury drop electrode.

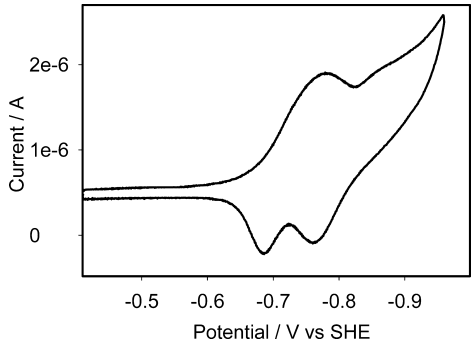

Figure 3. Cyclic voltammogram of complex **2b** in a 1.0 M pH 7.0 phosphate buffer. Conditions: scan rate, 100 mV s^{-1}; working electrode, mercury; counter electrode, Pt wire; reference electrode, aqueous Ag/AgCl.

reduction. The formation of $Co^{III}H$ species from the protonation of Co^{I} has been proposed as a key intermediate in the catalytic production of H_2 by Co complexes.[3f,7,25] Under the same conditions, **1b** displays redox potentials at −0.84 and −0.96 V (vs SHE), corresponding to $Co^{II/I}$ and $Co^{III}H/Co^{II}H$, respectively (Figure S7 in the SI). Therefore, the replacement of pyridyls with isoquinoline groups results in positive shifts of 110 and 140 mV for $Co^{II/I}$ and the proposed $Co^{III}H/Co^{II}H$, respectively. The more negative potentials of the $Co^{III}H/Co^{II}H$ couples than those of the $Co^{II/I}$ couples of both **1b** and **2b** are consistent with the potentials obtained from DFT computations (Table 1). When the Co complex is reduced, the gained electron delocalizes over both Co and a ligand scaffold to yield a structure with lower energy. The different effects of isoquinoline groups on the redox potentials of the Co complex **2b** result from the different distributions of the gained electron on the whole structure. While the $Co^{III/II}$ couple may be more metal-based, there could be more contribution of the ligand in the delocalization of added electrons in both the $Co^{II/I}$ and $Co^{III}H/Co^{II}H$ (or $Co^{I/0}$) couples.

The electrocatalytic production of H_2 by **2b** was investigated using a mercury pool as the working electrode in an H-type electrochemical cell.[8b] As shown in Figure 4, the cathodic scan of **2b** in 1.0 M sodium phosphate buffer at pH 7 shows an onset potential at −0.90 V (vs SHE) with the simultaneous formation of gas bubbles, suggesting electrocatalytic production of H_2. No significant current was observed at potentials more positive than −1.5 V vs SHE in the absence of **2b** (Figure 4). Under the same conditions, **1b** displays a lower current intensity than that of **2b**, demonstrating that **2b** exhibits higher activity for the electrolytic production of H_2 (Figure 4). When a controlled-growth mercury electrode was used as the working electrode, we observed similar higher activity of **2b** compared to **1b** (Figure S8 in the SI). The onset potential (−0.90 V vs SHE) for **2b** is more negative than the redox potential of the proposed $Co^{III}H/Co^{II}H$ couple (−0.82 V vs SHE), indicating

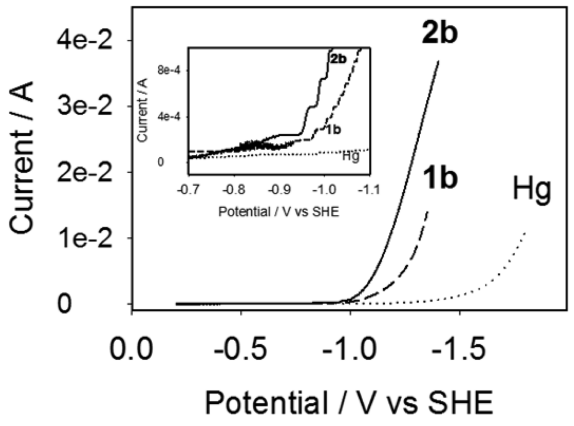

Figure 4. Cathodic scan of a 1.0 M sodium phosphate buffer at pH 7.0 in the presence of 50 μM **1b** (dashed line) or **2b** (solid line) and in the absence of catalyst (dotted line) (inset showing the enlarged window). Conditions: scan rate, 100 mV s^{-1}; working electrode, mercury pool; counter electrode, Pt mesh; reference electrode, aqueous Ag/AgCl.

that the formation of $Co^{II}H$ may be required before H_2 evolution.[26]

Overpotential for H_2 Production. The overpotential for the production of H_2 is an important parameter to evaluate the performance of various catalysts. However, there are no established standard protocols to determine the overpotentials for H_2 production by molecular catalysts. Reported in the literature, there have been a number of different ways to determine the overpotential for catalytic H_2 evolution, including the use of onset, the half-maximum intensity, or the peak potentials of a catalytic wave.[27] From the charge buildup over 200 s of bulk electrolysis at various potentials for H_2 production by **1b**, there is very little H_2 production at overpotentials less than 550 mV, while a significant amount of H_2 production could be observed at an overpotential of 600 mV.[8b] Following the same protocol, we carried out bulk electrolysis for H_2 production by **2b** under the same conditions as those of **1b**. As shown in Figure S9 in the SI, no significant amount of H_2 production could be observed at overpotentials less than 480 mV (−0.90 V vs SHE), and there is clearly H_2 production at an overpotential of 530 mV (Figure S9 in the SI). In a comparison to **1b**, which catalyzes H_2 production at an overpotential of 600 mV, the substitution of pyridyls with isoquinoline groups in **2b** results in a significant decrease of 70 mV in the overpotential for H_2 evolution in neutral aqueous solution.[8b]

The current efficiency of H_2 production by **2b** was examined from bulk electrolysis of 50 μM **2b** at room temperature in a 1.0 M phosphate buffer at pH 7. At controlled potentials of −1.4 and −1.3 V (vs SHE), the Faradaic efficiencies were determined to be 99 ± 1% and 98 ± 1%, respectively, the same as those obtained for complex **1b** under identical conditions (Table S2 in the SI). When controlled potential electrolysis was carried out at −1.2 V, **2b** shows a slightly lower current efficiency of 96 ± 1%, while **1b** shows a considerable decrease to 84 ± 2%, suggesting that **2b** is a more efficient catalyst for electrolytic H_2 production than complex **1b** at lower applied potentials (Table S3 in the SI). From the consumed charges over 1 h of bulk electrolysis in the presence of 50 μM **2b** at −1.2 V (vs SHE) in a 1.0 M phosphate buffer at pH 7, the rate for the evolution of H_2 by **2b** was calculated to be 1500 L of H_2 (mol of cat)$^{-1}$ h^{-1} (cm^2 Hg)$^{-1}$ (Figure 5) or a turnover number

dx.doi.org/10.1021/ic500840e | Inorg. Chem. 2014, 53, 10094−10100

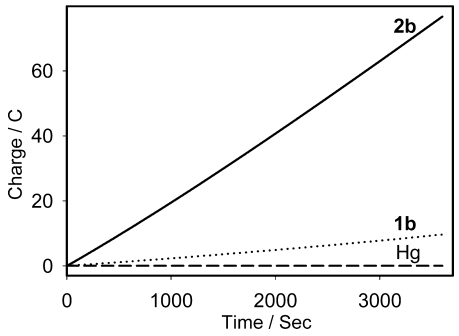

Figure 5. Controlled potential electrolysis at −1.2 V (vs SHE) in the presence of 50 μM **1b** (dotted line) or **2b** (solid line) and in the absence of catalyst (long dashed line) in a 1.0 M sodium phosphate buffer solution at pH 7.0. Condions: working electrode, mercury pool; counter electrode, Pt mesh; reference electrode, aqueous Ag/AgCl.

(TON) of >300 mol of H_2 (mol of cat)$^{-1}$. Under the same conditions, the rate of the evolution of H_2 by **1b** was calculated to be 160 L of H_2 (mol of cat)$^{-1}$ h^{-1} (cm^2 Hg)$^{-1}$ (Figure 5), or a TON of 30 mol of H_2 (mol of cat)$^{-1}$. Therefore, **2b** is 9 times as fast as **1b** in electrocatalytic proton reduction in neutral aqueous solution at an applied potential of −1.2 V (vs SHE). When the controlled potential was conducted at −1.4 V (vs SHE) in a 1.0 M phosphate buffer at pH 7, the rate for H_2 evolution by **2b** was calculated to be 4100 L of H_2 (mol of cat)$^{-1}$ h^{-1} (cm^2 Hg)$^{-1}$, or a TON of 890 mol of H_2 (mol of cat)$^{-1}$. Under the same conditions, we obtained a rate of 1800 L of H_2 (mol of cat)$^{-1}$ h^{-1} (cm^2 Hg)$^{-1}$ for the evolution of H_2 and a TON of 400 for **1b** during the first 1 h of electrolysis, demonstrating that complex **2b** is 2.2 times as fast as **1b** at an applied potential of −1.4 V (vs SHE; Figure S10 in the SI). As shown in Figure S11 in the SI, complex **2b** remains active for more than 5 h in bulk electrolysis at −1.4 V vs SHE without a significant decrease in activity, while complex **1b** is active for ∼3 h, suggesting that **2b** is a more stable catalyst than **1b** in electrolytic H_2 production. The higher stability of **2b** compared to **1b** could result from the more conjugated isoquinoline groups that help to stabilize the lower valent Co center in **2b** compared to **1b**.

Photochemical Studies. Photocatalytic H_2 production by **2b** was conducted following the literature method using ascorbic acid (0.1 M) as the electron donor and $[Ru(bpy)_3]^{2+}$ (0.5 mM) as the photosensitizer.[8b] Previous studies have shown the effects of pH on the activity of H_2 production when ascorbic acid was used as the electron donor, with an optimal pH of 4 for photocatalytic H_2 production by **1b**.[8b,c,28] The influence of the pH on the activity of H_2 evolution by **2b** was investigated in the pH range of 3−7. As shown in Figure S12 in the SI, the best pH for photocatalytic H_2 evolution by **2b** (5.0 μM) was observed at pH 5, with a TON of 1690 mol of H_2 (mol of cat)$^{-1}$. In order to determine if nanoparticles produced from the decomposition of **2b** are responsible for the activity of H_2 evolution, we added 1 mL of mercury to the reaction flask containing 10 mL of reaction solution in an acetate buffer at pH 5.0. As shown in Figure S13 in the SI, the addition of mercury results in no significant change in the photocatalytic production of H_2 by **2b**, suggesting that **2b** is a molecular catalyst for H_2 production.

Under neutral conditions, **2b** (5.0 μM) catalyzes H_2 production with a TON of 830 in a 1.0 M phosphate buffer at pH 7.0, ∼2 times that produced by **1b** (390) under the same conditions (Figure 6). Therefore, **2b** is a more active catalyst than **1b** for photocatalytic H_2 production under neutral aqueous conditions (Figure 6).

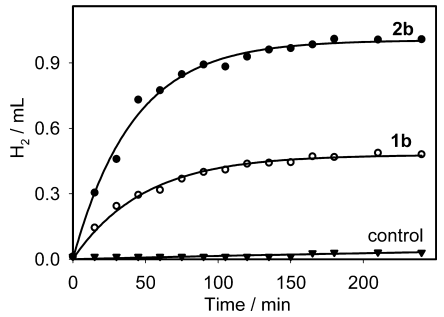

Figure 6. Photocatalytic H_2 production over time in a 1.0 M phosphate buffer at pH 7.0 with 0.1 M ascorbic acid, 0.5 mM $[Ru(bpy)_3]^{2+}$, with 5.0 μM **1b** (open circle) and **2b** (solid circles) and a control experiment in the absence of catalyst (solid triangle).

Our previous study showed that the photocatalytic activity of H_2 production by **1b** depends heavily on the concentration of **1b**, with increased TONs at lower concentrations of **1b**.[8b] To investigate the concentration effect on H_2 production, we carried out photolysis at different concentrations of **2b** ranging from 0.5 to 50 μM at pH 5.0. As shown in Figure S14 in the SI, **2b** catalyzes H_2 production with a TON of ∼600 mol of H_2 (mol of cat)$^{-1}$ at 50 μM **2b**. When the concentration of **2b** was lowered to 0.5 μM, the TON increased significantly to 5400 mol of H_2 (mol of cat)$^{-1}$, suggesting that the concentration of **2b** also has a significant effect on the photocatalytic activity for H_2 production (Figure S14 in the SI).

We have shown before that both **1b** and a photosensitizer are required to resume photocatalytic H_2 production after cessation of the H_2 evolution process.[8b] As observed in the case of **1b**, no significant amount of H_2 was produced after the addition of either **2b** or $[Ru(bpy)_3]^{2+}$ in the same amount as that used in the photocatalytic reaction. Both **2b** and $[Ru(bpy)_3]^{2+}$ are required to resume activity for H_2 production, suggesting the decomposition of both **2b** and $[Ru(bpy)_3]^{2+}$ during photolysis (Figure S15 in the SI).

To provide insight into the process of decomposition during photolysis, we monitored the photocatalytic H_2 production catalyzed by **1b** using mass spectroscopy. As shown in Figure S16a in the SI, the ESI-MS spectrum of the photolysis solution before irradiation (0 min) shows peaks at m/z 285.08, corresponding to $[Ru(bpy)_3]^{2+}$ (calcd m/z 285.06), and peaks at m/z 461.17 and 485.16, corresponding to the chloride-bound form of $[Co(DPA\text{-}Bpy)(Cl)]^+$ (calcd m/z 461.06) and the acetate-bound species of $[Co(DPA\text{-}Bpy)(OAc)]^+$ (calcd m/z 485.13), respectively. During the course of photolysis, a new peak at m/z 473.17 continues to increase in intensity (Figure S16b in the SI, 60 min). The peak at m/z 473.17 is consistent with the formation of $[Ru(bpy)_2(OAc)]^+$ (calcd m/z 473.06) species, resulting from the replacement of bpy by an acetate ion. During photolysis, the substitution of bpy in $[Ru(bpy)_3]^{2+}$ by an acetate ion, leading to the formation of $[Ru(bpy)_2(OAc)]^+$ species, has been reported as a major pathway for the photodecomposition of $[Ru(bpy)_3]^{2+}$.[29] After 150 min of photolysis, the peak at m/z 473.17 appeared with the highest intensity (Figure S16d in the SI), suggesting the formation of $[Ru(bpy)_2(OAc)]^+$ as the main reason for decomposition of the $[Ru(bpy)_3]^{2+}$ photosensitizer.

dx.doi.org/10.1021/ic500840e | Inorg. Chem. 2014, 53, 10094−10100

Scheme 3. Proposed Mechanism for Proton Reduction Catalyzed by 2b

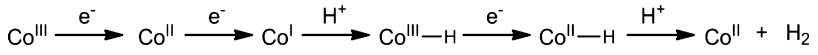

Over the course of photolysis, the peaks at m/z 461.17 and 485.16 also decreased in intensity. Before photolysis, while there is a tiny (negligible) peak at m/z 368.17 assigned to the free ligand DPA-Bpy (calcd m/z 368.19; the molecular mass of DPA-Bpy is 367.19), the intensity of the m/z 368.17 peak continues to increase over time (120 and 150 min in parts c and d of Figure S16 in the SI, respectively), suggesting dissociation of the Co ion from the DPA-Bpy scaffold. After 150 min of photolysis, the peak of DPA-Bpy has much higher intensity than the Co complexes at m/z 461.17 and 485.17 (Figure S16a in the SI). Therefore, dissociation of the Co ion from the ligand scaffold may be the main reason for catalyst decomposition during photolysis. We obtained similar results for the decomposition process of H_2 evolution catalyzed by **2b**.

Catalytic Mechanism. Over the past several years, a number of mechanisms have been proposed to account for the catalytic production of H_2 by Co complexes.[3f,4b,6a,f,7,25a,26a] We have carried out DFT computations to provide insight into the possible mechanism for H_2 production catalyzed by **2b**. From the calculated structures of possible intermediates involved in H_2 evolution (Tables S4 and S5 in the SI), we investigated the thermodynamic free-energy changes of eight possible mechanisms (Scheme S1 in the SI), showing that all paths are possible (Figure S17 in the SI). Electrochemical studies of H_2 evolution by **2b** have shown that the onset potential for the formation of H_2 lies after the redox event following the formation of Co^I species, which we tentatively assigned as the reduction of $Co^{III}H$ to $Co^{II}H$ (Figure 3). Scheme 3 shows a plausible mechanism for H_2 evolution by **2b**, involving the reduction of Co^{II} to yield the Co^I species and the formation of $Co^{III}H$ from the binding of a proton to Co^I. Further reduction of $Co^{III}H$ to $Co^{II}H$, followed by the binding of another proton, leads to the evolution of H_2 and regeneration of Co^{II} species.

During the catalytic evolution of H_2, reduction of the Co center and the binding of protons to the reduced Co center are key steps in determining the overpotential and TOF for H_2 evolution by Co complexes. While structural modifications of the ligand scaffold could result in Co centers with more positive reduction potentials favorable for reduction, the resulting reduced Co species are less favorable for protonation reactions, e.g., the binding of a proton to Co^I and the subsequent protonation of $Co^{II}H$ species shown in Scheme 3. Because of the opposite effects between the redox potentials and the basicity of the metal centers, previous studies on the structure–function relationship of metal catalysts for H_2 production have shown that tuning of the redox potentials of the metal centers through ligand modifications results in very little change in the overpotential for H_2 production.[6c] Metal catalysts with more positive reduction potentials require stronger acids for protonation and the evolution of H_2 because the metal centers are less nucleophilic with more positive reduction potentials.[5,6f] An electrochemical study of the redox potentials of **1b** and **2b** demonstrated that the replacement of pyridyls in **1b** with isoquinoline groups in **2b** leads to a positive shift of 110 mV for the $Co^{II/I}$ couple and 140 mV for the proposed $Co^{III}H/Co^{II}H$ couple, a favorable result for reduction of the metal centers, therefore, with lower overpotential for H_2 production. The pK_a study of **2b** and **1b** showed that the pK_a value of the coordinated Co–OH_2 in **2b** (5.9) is higher than that of **1b** (5.0), suggesting that the Co center in **2b** is more nucleophilic than that of **1b** and therefore favorable for the binding of a proton to the reduced Co center. Because of the more basic isoquinoline groups in **2b**, the $Co^{II}H$ intermediate of **2b** may be more basic and more favorable for protonation than the $Co^{II}H$ species of **1b**, explaining why **2b** has a lower overpotential and a faster rate in the evolution of H_2 than **1b**.

CONCLUSIONS

In conclusion, we have demonstrated that the replacement of pyridyls in DPA-Bpy with isoquinoline groups in DIQ-Bpy results in positive shifts of the redox potentials of the Co center in **2b** and a significant improvement in catalytic H_2 evolution under neutral conditions. Compared to **1b**, **2b** catalyzes the evolution of H_2 with lower overpotential, higher TON and TOF, and increased stability in the electrolytic production of H_2. Further detailed mechanistic studies of H_2 production catalyzed by **2b** and the modification of the ligand scaffold to optimize the activity for H_2 evolution are in progress.

ASSOCIATED CONTENT

Supporting Information

UV–vis, NMR, and ESI-MS spectra, pH titration of **2b**, cyclic voltammograms, Pourbaix diagram, photocatalytic H_2 evolution at various concentrations of **2b**, controlled potential electrolysis, the pH effect on photocatalytic H_2 evolution with **2b**, DFT-computed structures of possible intermediates of **2b**, Cartesian coordinates, and relative reaction free-energy change diagrams. This material is available free of charge via the Internet at http://pubs.acs.org.

AUTHOR INFORMATION

Corresponding Authors

*E-mail: ewebster@chemistry.msstate.edu.
*E-mail: xzhao1@memphis.edu.

Present Address

‡(G.L., C.E.W.) Department of Chemistry, Mississippi State University, Mississippi State, Mississippi 39762-9573, United States.

Notes

The authors declare no competing financial interest.

ACKNOWLEDGMENTS

We thank the Department of Chemistry at The University of Memphis. We acknowledge financial support from FedEx Institute of Technology and NSF EPS 1004083 (to X.Z.), Grant CHE 0955723 (to C.E.W.), and Grant CHE 0911528 (to C.E.W.). We also thank Dr. Truc Chi Pham for help with NMR and the LCQ Advantage liquid chromatograph–mass spectrometer. We appreciate the comments and suggestions to this manuscript from one reviewer.

REFERENCES

(1) (a) Lewis, N. S.; Nocera, D. G. *Proc. Natl. Acad. Sci. U. S. A.* **2006**, *103*, 15729–15735. (b) Gray, H. B. *Nat. Chem.* **2009**, *1*, 7–7.

(2) (a) Wang, M.; Chen, L.; Sun, L. C. *Energy Environ. Sci.* **2012**, *5*, 6763–6778. (b) Du, P.; Eisenberg, R. *Energy Environ. Sci.* **2012**, *5*, 6012–6021. (c) DuBois, D. L.; Bullock, R. M. *Eur. J. Inorg. Chem.*

2011, *2011*, 1017−1027. (d) Sutin, N.; Creutz, C.; Fujita, E. *Comments Inorg. Chem.* **1997**, *19*, 67−92. (e) Rose, M. J.; Gray, H. B.; Winkler, J. R. *J. Am. Chem. Soc.* **2012**, *134*, 8310−8313. (f) Tong, L.; Zong, R.; Thummel, R. P. *J. Am. Chem. Soc.* **2014**, *136*, 4881−4884.

(3) (a) Sun, Y.; Bigi, J. P.; Piro, N. A.; Tang, M. L.; Long, J. R.; Chang, C. J. *J. Am. Chem. Soc.* **2011**, *133*, 9212−9215. (b) Sun, Y.; Sun, J.; Long, J. R.; Yang, P.; Chang, C. J. *Chem. Sci.* **2013**, *4*, 118−124. (c) Chen, L.; Wang, M.; Han, K.; Zhang, P.; Gloaguen, F.; Sun, L. *Energy Environ. Sci.* **2014**, *7*, 329−334. (d) Stubbert, B. D.; Peters, J. C.; Gray, H. B. *J. Am. Chem. Soc.* **2011**, *133*, 18070−18073. (e) Zhang, P.; Wang, M.; Gloaguen, F.; Chen, L.; Quentel, F.; Sun, L. *Chem. Commun.* **2013**, *49*, 9455−9457. (f) Singh, W. M.; Mirmohades, M.; Jane, R. T.; White, T. A.; Hammarstrom, L.; Thapper, A.; Lomoth, R.; Ott, S. *Chem. Commun.* **2013**, *49*, 8638−8640. (g) Bachmann, C.; Guttentag, M.; Spingler, B.; Alberto, R. *Inorg. Chem.* **2013**, *52*, 6055−6061. (h) Kleingardner, J. G.; Kandemir, B.; Bren, K. L. *J. Am. Chem. Soc.* **2013**, *136*, 4−7.

(4) (a) Bigi, J. P.; Hanna, T. E.; Harman, W. H.; Chang, A.; Chang, C. J. *Chem. Commun.* **2010**, *46*, 958−960. (b) King, A. E.; Surendranath, Y.; Piro, N. A.; Bigi, J. P.; Long, J. R.; Chang, C. J. *Chem. Sci.* **2013**, *4*, 1578−1587.

(5) Artero, V.; Chavarot-Kerlidou, M.; Fontecave, M. *Angew. Chem., Int. Ed.* **2011**, *50*, 7238−7266.

(6) (a) Razavet, M.; Artero, V.; Fontecave, M. *Inorg. Chem.* **2005**, *44*, 4786−4795. (b) Wakerley, D. W.; Reisner, E. *Phys. Chem. Chem. Phys.* **2014**, *16*, 5739−5746. (c) Collman, J. P.; Ha, Y.; Wagenknecht, P. S.; Lopez, M. A.; Guilard, R. *J. Am. Chem. Soc.* **1993**, *115*, 9080−9088. (d) Artero, V.; Fontecave, M. *Coord. Chem. Rev.* **2005**, *249*, 1518−1535. (e) Toscano, P. J.; Swider, T. F.; Marzilli, L. G.; Bresciani-Pahor, N.; Randaccio, L. *Inorg. Chem.* **1983**, *22*, 3416−3421. (f) Baffert, C.; Artero, V.; Fontecave, M. *Inorg. Chem.* **2007**, *46*, 1817−1824.

(7) Hu, X.; Brunschwig, B. S.; Peters, J. C. *J. Am. Chem. Soc.* **2007**, *129*, 8988−8998.

(8) (a) Radaram, B.; Ivie, J. A.; Grudzien, R. M.; Reibenspies, J. H.; Webster, C. E.; Zhao, X. *Inorg. Chem.* **2011**, *50*, 10564−10571. (b) Singh, W. M.; Baine, T.; Kudo, S.; Tian, S.; Ma, X. A. N.; Zhou, H.; DeYonker, N. J.; Pham, T. C.; Bollinger, J. C.; Baker, D. L.; Yan, B.; Webster, C. E.; Zhao, X. *Angew. Chem., Int. Ed.* **2012**, *51*, 5941−5944. (c) Shan, B.; Baine, T.; Ma, X. A. N.; Zhao, X.; Schmehl, R. H. *Inorg. Chem.* **2013**, *52*, 4853−4859.

(9) (a) Albert, A.; Phillips, J. N. *J. Chem. Soc.* **1956**, 1294−1304. (b) Hosmane, R.; Liebman, J. *Struct Chem.* **2009**, *20*, 693−697.

(10) (a) Tyeklar, Z.; Jacobson, R. R.; Wei, N.; Murthy, N. N.; Zubieta, J.; Karlin, K. D. *J. Am. Chem. Soc.* **1993**, *115*, 2677−2689. (b) Gultneh, Y.; Yisgedu, T. B.; Tesema, Y. T.; Butcher, R. J. *Inorg. Chem.* **2003**, *42*, 1857−1867. (c) Murashima, T.; Tsukiyama, S.; Fujii, S.; Hayata, K.; Sakai, H.; Miyazawa, T.; Yamada, T. *Org. Biomol. Chem.* **2005**, *3*, 4060−4064.

(11) Heintz, R. A.; Smith, J. A.; Szalay, P. S.; Weisgerber, A.; Dunbar, K. R. *Inorg. Synth.* **2002**, *33*, 75−83.

(12) Vennampalli, M.; Liang, G.; Webster, C. E.; Zhao, X. *Eur. J. Inorg. Chem.* **2014**, 715−721.

(13) Connelly, N. G.; Geiger, W. E. *Chem. Rev.* **1996**, *96*, 877−910.

(14) (a) Perdew, J. P.; Burke, K.; Ernzerhof, M. *Phys. Rev. Lett.* **1996**, *77*, 3865−3868. (b) Perdew, J. P.; Burke, K.; Ernzerhof, M. *Phys. Rev. Lett.* **1997**, *78*, 1396.

(15) Frisch, M. J., et al. *Gaussian 09*, revision C.01; Gaussian, Inc.: Wallingford, CT, 2009.

(16) (a) Hay, P. J.; Wadt, W. R. *J. Chem. Phys.* **1985**, *82*, 299−310. (b) Couty, M.; Hall, M. B. *J. Comput. Chem.* **1996**, *17*, 1359−1370.

(17) (a) Hehre, W. J.; Ditchfie, R.; Pople, J. A. *J. Chem. Phys.* **1972**, *56*, 2257−2261. (b) Hariharan, P. C.; Pople, J. A. *Theor. Chim. Acta* **1973**, *28*, 213−222. (c) Foresman, J. B.; Frisch, Æ. *Exploring Chemistry with Electronic Structure Methods*, 2nd ed.; Gaussian, Inc.: Pittsburgh, PA, 1996; p 110.

(18) The 6-31G(d′) basis set has the d polarization functions for C, N, and O taken from the 6-311G(d) basis sets, instead of the original arbitrarily assigned value of 0.8 used in the 6-31G(d) basis sets.

(19) Marenich, A. V.; Cramer, C. J.; Truhlar, D. G. *J. Phys. Chem. B* **2009**, *113*, 6378−6396.

(20) (a) Kim, H.; Park, J.; Lee, Y. S. *J. Comput. Chem.* **2013**, *34*, 2233−2241. (b) Baik, M.-H.; Friesner, R. A. *J. Phys. Chem. A* **2002**, *106*, 7407−7412.

(21) (a) Kelly, C. P.; Cramer, C. J.; Truhlar, D. G. *J. Phys. Chem. B* **2006**, *111*, 408−422. (b) Kelly, C. P.; Cramer, C. J.; Truhlar, D. G. *J. Phys. Chem. B* **2006**, *110*, 16066−16081.

(22) Moser, A.; Range, K.; York, D. M. *J. Phys. Chem. B* **2010**, *114*, 13911−13921.

(23) Xie, J.; Zhou, Q.; Li, C.; Wang, W.; Hou, Y.; Zhang, B.; Wang, X. *Chem. Commun.* **2014**, *50*, 6520−6522.

(24) (a) Delahay, P.; Pourbaix, M.; Van Rysselberghe, P. *J. Chem. Educ.* **1950**, *27*, 683. (b) Barnum, D. W. *J. Chem. Educ.* **1982**, *59*, 809.

(25) (a) Marinescu, S. C.; Winkler, J. R.; Gray, H. B. *Proc. Natl. Acad. Sci. U. S. A.* **2012**, *109*, 15127−15131. (b) Schneider, J.; Jia, H.; Muckerman, J. T.; Fujita, E. *Chem. Soc. Rev.* **2012**, *41*, 2036−2051.

(26) (a) Muckerman, J. T.; Fujita, E. *Chem. Commun.* **2011**, *47*, 12456−12458. (b) Dempsey, J. L.; Winkler, J. R.; Gray, H. B. *J. Am. Chem. Soc.* **2010**, *132*, 16774−16776. (c) Solis, B. H.; Hammes-Schiffer, S. *Inorg. Chem.* **2011**, *50*, 11252−11262.

(27) Fourmond, V.; Jacques, P.-A.; Fontecave, M.; Artero, V. *Inorg. Chem.* **2010**, *49*, 10338−10347.

(28) (a) McNamara, W. R.; Han, Z.; Alperin, P. J.; Brennessel, W. W.; Holland, P. L.; Eisenberg, R. *J. Am. Chem. Soc.* **2011**, *133*, 15368−15371. (b) Wang, F.; Wang, W.-G.; Wang, X.-J.; Wang, H.-Y.; Tung, C.-H.; Wu, L.-Z. *Angew. Chem., Int. Ed.* **2011**, *50*, 3193−3197.

(29) Vaidyalingam, A.; Dutta, P. K. *Anal. Chem.* **2000**, *72*, 5219−5224.